PHYSICAL REVIEW B **90**, 214423 (2014)

Magnetic structure and magnetocalorics of $GdPO_4$

E. Palacios,[1,*] J. A. Rodríguez-Velamazán,[1,2] M. Evangelisti,[1] G. J. McIntyre,[2,3] G. Lorusso,[1] D. Visser,[4,5] L. J. de Jongh,[6] and L. A. Boatner[7]

[1]*Instituto de Ciencia de Materiales de Aragón (ICMA) and Departamento de Física de la Materia Condensada, CSIC–University of Zaragoza, Pedro Cerbuna 12, 50009 Zaragoza, Spain*

[2]*Institut Laue-Langevin (ILL), 71 Avenue des Martyrs, 38000 Grenoble, France*

[3]*Australian Nuclear Science and Technology Organisation, Lucas Heights, NSW 2234, Australia*

[4]*ISIS Facility, Rutherford Appleton Laboratory, Chilton, Didcot OX11 0QX, United Kingdom*

[5]*Department Radiation, Radionuclides & Reactors, Section FAME, Delft University of Technology, NL-2629 JB Delft, The Netherlands*

[6]*Kamerlingh Onnes Laboratory, Leiden University, NL-2300 RA Leiden, The Netherlands*

[7]*Center for Radiation Detection Materials and Systems, Materials Science and Technology Division, Oak Ridge National Laboratory, Oak Ridge, Tennessee 37831-6056, USA*

(Received 21 October 2014; revised manuscript received 14 November 2014; published 12 December 2014)

The magnetic ordering structure of $GdPO_4$ is determined at $T = 60$ mK by the diffraction of hot neutrons with wavelength $\lambda = 0.4696$ Å. It corresponds to a noncollinear antiferromagnetic arrangement of the Gd moments with propagation vector $\mathbf{k} = (1/2,0,1/2)$. This arrangement is found to minimize the dipole-dipole interaction and the crystal-field anisotropy energy, the magnetic superexchange being much smaller. The intensity of the magnetic reflections decreases with increasing temperature and vanishes at $T \approx 0.8$ K, in agreement with the magnetic ordering temperature $T_N = 0.77$ K, as reported in previous works based on heat capacity and magnetic susceptibility measurements. The magnetocaloric parameters have been determined from heat capacity data at constant applied fields up to 7 T, as well as from isothermal magnetization data. The magnetocaloric effect, for a field change $\Delta B = 0 - 7$ T, reaches $-\Delta S_T = 375.8$ mJ/cm^{3}K^{-1} at $T = 2.1$ K, largely exceeding the maximum values reported to date for Gd-based magnetic refrigerants.

DOI: 10.1103/PhysRevB.90.214423 PACS number(s): 61.05.fg, 75.30.Sg, 75.50.Ee

I. INTRODUCTION

Adiabatic demagnetization of a paramagnetic salt was the first technology applied to obtain temperatures below 0.5 K [1]. Today, temperatures of 2 mK can be attained routinely by this procedure [2]. For this purpose compounds with a large magnetic moment and extremely low ordering temperatures are used, e.g., gadolinium gallium garnet [3] or cerium magnesium nitrate, which contain a large fraction of inert atoms to prevent magnetic ordering by the exchange or dipole-dipole interactions. In the sixties, the newly developed technology of ^{3}He/^{4}He dilution refrigeration, by which low temperatures can be maintained continuously, gradually replaced adiabatic demagnetization as the main method to reach temperatures between 20 mK and 1 K. Nevertheless, adiabatic demagnetization remained an option for refrigeration, especially in cases where the use of fluids is not convenient (e.g., in gravity-free spacecrafts). Moreover, since the rare and strategically important ^{3}He isotope is increasingly expensive, the adiabatic demagnetization technique is becoming competitive again. In the present context, the method is also used for cooling in the liquid-helium temperature range above 1 K, for which compounds with large magnetization under field, low magnetic anisotropy and low magnetic ordering temperatures are desirable. The first and the third conditions are antagonistic to each other since, by separating the magnetic atoms far enough to decrease the dipole-dipole interaction, the magnetic density decreases likewise. However, the dipolar interaction can still be reduced to produce ordering well below 1 K by choosing compounds with special crystal structures. For instance, this can be accomplished if the magnetic ions are at short distances in a so-called "frustrated" arrangement, thus leaving the small magnetic anisotropy and large magnetic density as the only ingredients. A valid example is gadolinium formate, $Gd(HCOO)_3$, a magnetically dense metal-organic framework material that has recently proved to be a good candidate, reaching a record magnetocaloric effect (MCE) between ca. 1 K and 5 K [4], with a maximum magnetic entropy decrease on isothermal magnetization $-\Delta S_T = 216.3$ mJ/cm^{3}K^{-1} at $T = 1.8$ K for an external field variation $\Delta B = 7$ T.

Anhydrous gadolinium phosphate, $GdPO_4$, appears to be another good candidate, since the ionic bonding prevents strong overlap of the Gd wave functions with its nearest neighbors (hence promoting weak exchange interactions) and the absence of an orbital moment implies a low magnetic anisotropy. This leads to a magnetic ordering temperature of only $T_N = 0.77$ K [5]. The magnetic dipolar density at saturation is $M_s = 155$ Am^{2}kg^{-1} or $\rho\mu_0 M_s = 1.2$ T, similar to that of permanent magnets. The magnetic entropy in the paramagnetic state, $S_m = R\ln(8) = 17.3$ Jmol^{-1}K^{-1} = 68.6 Jkg^{-1}K^{-1} = 416 Jcm^{-3}K^{-1}, suggests that its increase on demagnetization might be very high. This compound has been studied by heat capacity and magnetic susceptibility in the form of nanoparticles and in bulk, both for powder samples and single crystals [5,6]. Also Monte Carlo simulations were made [6]. The experiments indicated a compensated antiferromagnetic structure below T_N, interpreted as resulting from a competition between the dipolar, exchange, and anisotropy energies. Because of the lack of sufficiently detailed information, the data were analyzed in terms of a simple uniaxial two-sublattice antiferromagnet [6]. However,

*Corresponding author: elias@unizar.es

TABLE I. Structural parameters resulting from the refinements at 298 K and 60 mK. The space group is $P2_1/n$, with $Z = 4$ chemical units per cell. Fractional coordinates are in units of a, b, and c. Standard deviations in the last digit units are given in parentheses. $R_{\rm nucl}, R_{\rm mag} = \sum_{h,k,l} |F_{hkl}({\rm obs}) - F_{hkl}({\rm cal})|/|F_{hkl}({\rm obs})|$ for the nuclear and magnetic reflections, respectively. Similarly but with F^2 for $R(F^2)$. For more details see Supplemental Material [18].

T	Atom	x	y	z	$< U^2 >$ (Å^2)
298 K	Gd	0.2818(3)	0.1553(3)	0.0970(3)	0.0063(10)
	P	0.3028(6)	0.1608(6)	0.6130(7)	0.0077(12)
	O1	0.2502(5)	0.0030(6)	0.4371(6)	0.0097(11)
	O2	0.3833(6)	0.3359(5)	0.5025(6)	0.0103(11)
	O3	0.4735(5)	0.1023(5)	0.8117(6)	0.0089(11)
	O4	0.1218(6)	0.2105(5)	0.7122(6)	0.0089(12)
a,b,c(Å), $\beta(^\circ)$		6.6252(18)	6.8372(16)	6.3176(18)	104.017(12)
$R_{\rm nucl} = 0.06$	$wR_{\rm nucl}(F^2) = 0.11$	$N_{\rm obs}$, $I > 5\sigma = 215$ (unique)			
60 mK	Gd	0.2825(15)	0.154(5)	0.0995(19)	0
	μ(Gd)/μ_B	6.57(12)	2.0(3)	3.3(2)	
	P	0.305(3)	0.173(9)	0.610(3)	0
	O1	0.249(3)	0.000(8)	0.438(2)	0
	O2	0.379(3)	0.326(12)	0.504(2)	0
	O3	0.475(3)	0.114(10)	0.814(2)	0
	O4	0.119(3)	0.206(11)	0.712(3)	0
a,b,c(Å), $\beta(^\circ)$		6.625(4)	6.82	6.317(3)	104.06(3)
$R_{\rm nucl} = 0.07$	$R_{\rm mag} = 0.12$	$R_{\rm mag}(F^2) = 0.21$	$N_{\rm obs,mag}$, $I > 5\sigma = 105$		

the field-dependent susceptibility measurements on a single crystal as well as the Monte Carlo simulations did indicate the structure to be more complex. Accordingly, it was decided to investigate the magnetic structure by neutron diffraction on a single crystal, which formed the main motivation for the present paper.

In addition, we report and discuss new data obtained for the MCE of this material, i.e., the isothermal entropy increment (ΔS_T) and adiabatic temperature increment (ΔT_S) under given magnetic field variations, in both cases deduced from heat capacity measurements at constant fields (C_B vs T) up to 7 T, and for the first one also from isothermal magnetization (M_T vs B) measurements up to 5 T.

II. NEUTRON DIFFRACTION IN $GdPO_4$

A. Experimental

Single-crystal neutron diffraction was performed on the instrument D9 at the high-flux reactor of the Institut Laue-Langevin, using hot neutrons with a short wavelength $\lambda = 0.4696(2)$ Å, obtained from a Cu(220) monochromator and calibrated with a single crystal of Ge, by which the problem of severe absorption of thermal neutrons by natural Gd can be circumvented [7]. An indium filter was used to suppress the $\lambda/2$ contamination. The coherent scattering length for this wavelength has been interpolated from those given in Table I of Ref. [8], giving $b = (1.042 - 0.034{\rm i}) \times 10^{-12}$ cm. The absorption cross section was deduced from the imaginary part of the scattering length $-b''$ as $\sigma_a = 4\pi b''/k = 2b''\lambda = 319$ barn [9]. The inverse of the neutron mean-free path is given by $\Sigma_a = \sigma_a Z/V_{\rm cell} = 0.47\,{\rm mm}^{-1}$, where $V_{\rm cell} = 276.39$ Å^3 is the unit-cell volume and $Z = 4$ is the number of Gd atoms per unit cell. For the other elements, the coherent scattering lengths reported in the literature have been taken, i.e., $b_P = 5.130 \times 10^{-12}$ cm, $b_O = 5.803 \times 10^{-12}$ cm, similarly for the Gd magnetic form factor [9]. For this experiment, D9 was equipped with a small area detector of $64 \times 64\,{\rm mm}^2$ consisting of 1024 pixels at 40 cm from the sample [10], which allowed determination of the centroids of all observed reflections and optimal delineation of each peak from the background. The crystal was a platelet normal to the $(10\bar{1})$ crystal direction, 0.5 mm thick with face dimensions $1 \times 1.5\,{\rm mm}^2$.

A collection of 245 unique reflections was made at 298 K using the standard four-circle setup with an Eulerian cradle to orient the sample, in order to check the reported monazite-type structure solved by x-ray diffraction [11,12]. For the measurements below 1 K, the crystal was attached to the mixing chamber of a ^{3}He/^{4}He dilution cryostat which could only be rotated around the vertical axis. Normal-beam Weissenberg geometry, where the crystal can be rotated around the vertical laboratory axis with the detector rotating around vertical and horizontal axes, was used for data collection in this case. During the cooling process some strong reflections were followed, but no evident changes were observed below 10 K. At 60 mK q scans revealed magnetic satellites only at $(h \pm 1/2, k, l \pm 1/2)$, thus giving the propagation vector for the magnetic structure $\mathbf{k} = (1/2, 0, 1/2)$. 250 (71 observed) "nuclear" reflections with integer indices (hkl) and 359 (105 observed) "magnetic" reflections with half-odd h and l indices were scanned.

Finally, two strong magnetic reflections $(1.5, 0, -1.5)$ and $(0.5, -1, -2.5)$ were scanned at different temperatures between 60 mK and 1 K to track the evolution of the intensity with the temperature (Fig. 1). It vanishes near 0.80 K, consistent with the peak at $T_N = 0.77$ K, in heat capacity [5,6].

All data were corrected for background by the minimum $\sigma(I)/I$ algorithm [13] and the Lorentz correction appropriate to the particular scan geometry applied [14]. Correction for absorption and calculation of the mean path length for each reflection were carried out by Gaussian integration [15] with the program DATAP, using the calculated absorption cross

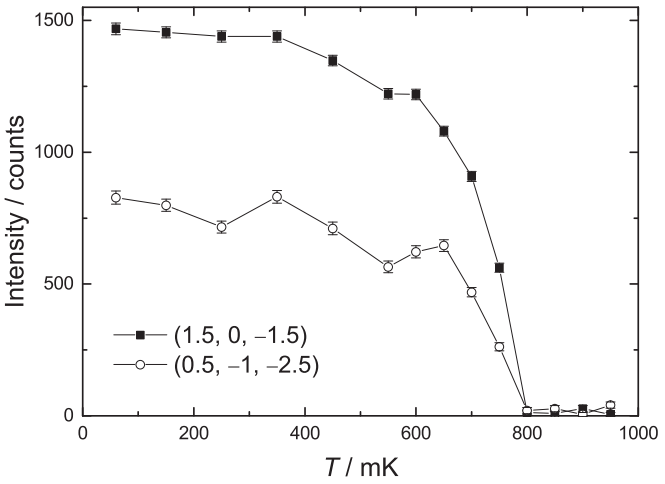

FIG. 1. Variation of the intensity of the strong magnetic reflections (1.5,0,−1.5) and (0.5,−1,−2.5) with temperature. Lines are guide to the eye.

section given above. Refinement of both the crystal and magnetic structure was made using the Fullprof Suite [16] in single-crystal mode.

B. Crystal structure at room temperature

The crystal structure at 298 K (data collection in the conventional four-circle configuration) was refined using the reported x-ray parameters as starting values [11,12]. No significant differences were found in the atomic coordinates with respect to those reported values. The most relevant (and even then very small) difference concerns the position of the O atoms. The P-O distances [1.530(1) Å on average] agree with usual values for this molecular group 1.54(2) Å [17]. The maximum departure of the O-P-O angle with respect to the ideal tetrahedral angle is 5.6°. The refinement parameters and reliability factors are shown in Table I. In spite of the higher R value than for the x-ray experiment, the obtained positions of the O and P atoms should be considered as more reliable than given in Refs. [11] and [12] (they claim $R = 0.031$ and 0.016, respectively), due to the stronger relative scattering amplitudes of these atoms for neutrons than for x rays, as compared with that of Gd. The most important error in our neutron diffraction experiment arises from the imprecise estimation of the intensities of some severely absorbed reflections with the incident or diffracted beam nearly parallel to the platelet. For instance among the most absorbed reflections, the observed $(\bar{2}02)$ is circa three times weaker than expected before applying the absorption correction and circa 30% weaker after such correction, this suggesting that the absorption can bias the results. The structural parameters are summarized in Table I and in the Supplemental Material [18].

C. Crystal and magnetic structures at 60 mK

As mentioned, a set of 71 unique reflections (hkl), with $k = 0,-1,-2$ and integer h and l indices was collected. The nuclear structure was refined starting with the positional parameters at $T = 298$ K, fixing the thermal parameters to zero. This resulted in very similar positional parameters as found at 298 K but with $R = 0.070$, indicating that the anisotropic thermal parameters at 298 K compensate to some extent for the disagreement between calculated and observed values due to other causes, especially absorption. The cell parameter b was not refined because the detector has a narrowly limited degree of freedom out of the equatorial plane. Consequently all reflections correspond to very small k values (2^{nd} Miller index), and the refinement of b is ill conditioned. Instead, a value of b was assumed, precise enough to center all scanned reflections. The main results of the refinement are displayed in Table I. Details of the refinement of the nuclear and magnetic structure refinements can be found in the Supplemental Material [18].

TABLE II. Magnetic irreducible representations for the position (x,y,z) in the space group $P2_1/n$ for $\mathbf{k} = (1/2,0,1/2)$. The atom 1 is at $(x,y,z) = (0.2825,0.154,0.0995)$. Atoms 2, 3 and 4 are obtained by the symmetry operations $2_1 = 1/2-x,1/2+y,1/2-z$, $\bar{1} = -x,-y-z$ and $n = 1/2+x,1/2-y,1/2+z$, respectively. The given combinations follow conventions similar to that of Bertaut [19]: $\mathbf{F} = \mathbf{s_1}+\mathbf{s_2}+\mathbf{s_3}+\mathbf{s_4}, \mathbf{G} = \mathbf{s_1}-\mathbf{s_2}+\mathbf{s_3}-\mathbf{s_4}, \mathbf{A} = \mathbf{s_1}+\mathbf{s_2}-\mathbf{s_3}-\mathbf{s_4}$ and $\mathbf{C} = \mathbf{s_1}-\mathbf{s_2}-\mathbf{s_3}+\mathbf{s_4}$. All irreducible representations are single dimensional. The sign of the transformation of the base vectors under each symmetry operation is given.

	1	2_1	$\bar{1}$	n	s_x	s_y	s_z
Γ_1	+	+	+	+	G_x	F_y	G_z
Γ_2	+	−	+	−	F_x	G_y	F_z
Γ_3	+	−	−	+	A_x	C_y	A_z
Γ_4	+	+	−	−	C_x	A_y	C_z

Some symmetry considerations were used to solve the magnetic structure. There are four Gd atoms in the unit cell. For $\mathbf{k} = (1/2,0,1/2)$ and for the space group $P2_1/n$, the irreducible magnetic representations (combinations of the spins which transform into themselves under the space operations) are given in Table II [19].

For $\mathbf{k} = (1/2,0,1/2)$, all magnetic reflections have half-odd h and l indices, and an integer k index, which allows us to deal with the magnetic and nuclear structures separately. Moreover for the group $P2_1/n$, some of the $(h0l)$ reflections are forbidden by the positional symmetry operations. The magnetic structure factor for these special reflections is

$$\mathbf{F}_{h0l} = \alpha f(q) \sum_j \mu_\perp \exp[2\pi i(hx_j + lz_j)], \qquad (1)$$

where $\alpha = 2.695 \times 10^{-12}$ cm$/\mu_B$ is the magnetic scattering length, μ_B the Bohr magneton, $f(q)$ the form factor for Gd, $\mu_\perp$ the projection of the magnetic moment (in Bohr magnetons) on the plane perpendicular to the scattering vector $\mathbf{q}$, and the sum runs over the four Gd atoms per unit cell. For a collinear structure, $\mathbf{F}_{h0l}$ can be written as

$$\begin{aligned}\mathbf{F}_{h0l} = \alpha f(q)\mu_\perp \times \{&\exp[2\pi i(hx+lz)] \\ &\times (e_1 + e_4 \cdot \exp[\pi i(h+l)]) \\ &+ \exp[-2\pi i(hx+lz)](e_3 + e_2 \cdot \exp[\pi i(h+l)])\}. \qquad (2)\end{aligned}$$

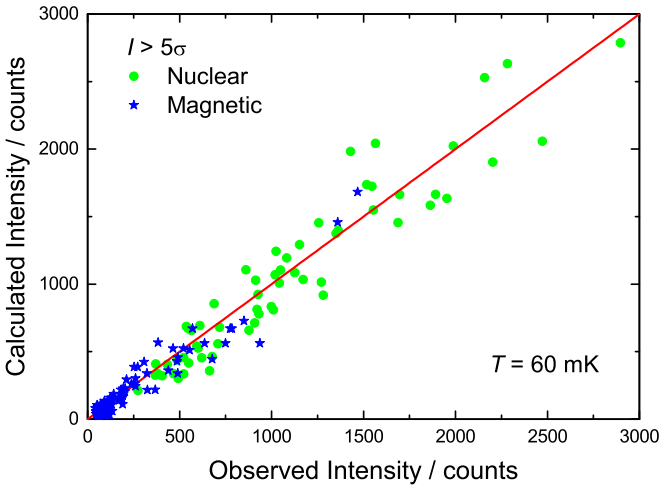

FIG. 2. (Color online) Plot of the observed vs calculated intensities for the ($I > 5\sigma$) magnetic and nuclear reflections.

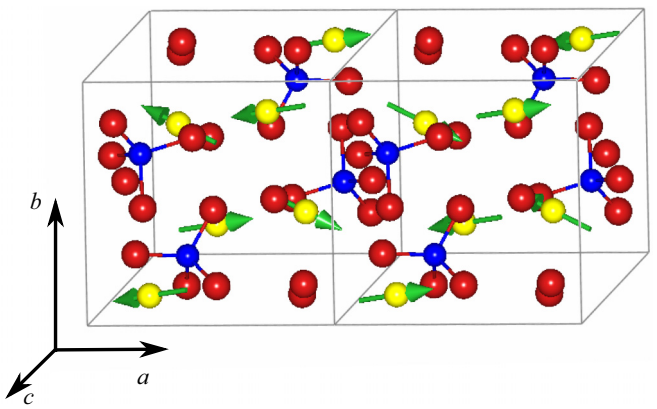

FIG. 3. (Color online) Nuclear and magnetic structure at $T = 60$ mK. Red: O, blue: P, yellow: Gd. Green arrows: moments of Gd.

where (x,y,z) are the coordinates of the reference Gd atom, as given in Table I and the parameters $e_j = +1$ or -1, ($j = 1,\ldots,4$) define the magnetic mode F, G, A, or C, i.e., $e_1 = e_4 = 1, e_2 = e_3 = -1$ for a C mode. For the F or C modes, $h + l$ must be even (similarly to the extinction produced by the glide plane n in the usual nuclear reflections), and for the G and A modes $h + l$ must be odd. Fifteen reflections ($h0l$) with h and l half odd were clearly observed with $h + l$ even though there were also five weaker reflections with $I > 5\sigma$ and $h + l$ odd, namely $(1/2,0,-7/2)$, $(3/2,0,-5/2)$, $(5/2,0,-7/2)$, $(7/2,0,-5/2)$, and $(5/2,0,1/2)$. The existence of both types of reflections implies a noncollinear structure. The occurrence of F modes is difficult to understand on physical grounds since all four moments would be parallel in one unit cell, but opposite to the moments in the nearest cells. Then, the plausible irreducible representations are $\Gamma_4 : C_x A_y C_z$ or $\Gamma_3 : A_x C_y A_z$.

According to the observed ($h0l$) reflections, in a first stage, we refined the moment direction assuming a collinear C mode with the moments lying in the xz plane, fixing the y component, $\mu_y = 0$. The least-squares procedure converged, giving the moment at an angle of nearly 30° to the x axis, which corresponds to the irreducible representation $\Gamma_4 : C_x A_y C_z$, with $\mu_y = 0$. Finally a refinement was made leaving μ_y free (keeping just three free parameters defining the Gd moment, i.e., the magnitude μ and the polar angles (θ,ϕ) defining the orientation of moment at site 1, all other moments being deduced by symmetry) and using the 105 magnetic reflections with $I > 5\sigma$. Here θ is the angle between the moments and the b axis, whereas ϕ is the angle between the projection of the moment on the ac plane and the c axis. The fit led to the moment parameters given in Table I, corresponding to $\theta = 73°$ and $\phi = 29°$. Moreover, this model predicts all scanned but unobserved reflections to be very weak, indeed. Figure 2 summarizes graphically the quality of the refinement of the magnetic structure, whereas Fig. 3 shows the nuclear and magnetic structures with the crystal b axis upwards.

In Ref. [6] the moments were assumed to lie near the ab plane, with c and b as the hardest and easiest directions, respectively (model $A_x C_y A_z$ with $\mu_z = 0$). However, this possibility is not compatible with the observed intensities in the neutron diffraction data. A refinement fixing the moment to lie in the ab plane gives a rather poor $R = 0.19$, considering all the 105 observed reflections with $I > 5\sigma$, with the two most disagreeable being $(-1.5,-1,0.5)$ ($I_{calc}/I_{obs} = 3$) and $(-0.5,-2,-1.5)$ ($I_{calc}/I_{obs} = 0.38$). In contrast, the most disagreeable reflections for the model proposed here $C_x A_y C_z$ (i.e., $(0.5,-1,-2.5)$, $I_{calc}/I_{obs} = 0.60$, $(2.5,-3,0.5)$, $I_{calc}/I_{obs} = 0.60$) correspond to strong reflections which could be affected by an imprecise correction of extinction. They have the same discrepancy for the "easy b direction" model. Also the modes $F_x G_y F_z$ and $G_x F_y G_z$ can be ruled out since many strong calculated intensities are actually observed as weak and vice versa.

III. HEAT CAPACITY AND MAGNETOCALORIC EFFECT

The heat capacity C_B at constant field was measured by the relaxation method in a PPMS device from Quantum Design, equipped with the ^{3}He option (Fig. 4, top panel). Our results agree with data in the literature [5,6,20]. In these publications, the data on $GdPO_4$ for $T \geqslant 15$ K were found to coincide with those of the nonmagnetic isomorph $LaPO_4$ and were analyzed in terms of a simple Debye model, giving the Debye temperature $\theta_D = 227$ K. Considering as relevant only the three acoustic modes in the temperature region where the magnetic contribution is negligible (Fig. 4), a fit of the experimental data to the Debye law for the phonon contribution, $C_{ph} = AT^3 = (12R\pi^4/5)(T/\theta_D)^3$ where R is the gas constant, yields the value $\theta_D = 211$ K for the Debye temperature, i.e., close to the previous estimate [5,6]. By subtracting C_{ph} from C_B, the magnetic contribution C_m to the heat capacity is obtained. Thus, by taking the integral $E = -\int_0^\infty C_m dT$, the energy involved in the magnetic ordering process can be calculated. This yields an experimental magnetic energy per particle of $E/k_B = -2.2(1)$ K (see also Fig. 6). We postpone a further analysis of the magnetic heat capacity to the discussion section and will now concentrate on the magnetocaloric effect, whose parameters can be deduced from it.

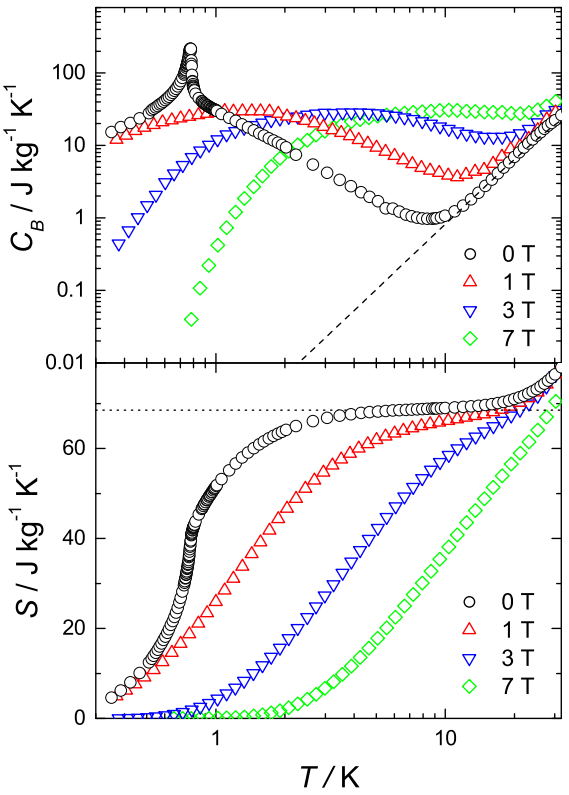

FIG. 4. (Color online) Top: Heat capacity at applied magnetic field $C_B(T)$. Dashed line: Calculation of the phonon contribution. Bottom: Entropy $S(T,B)$ deduced from heat capacity. Details in the text. Dotted line: infinite temperature limit for the molar magnetic entropy $S_m/R(\infty) = \ln(2s+1)$ for $s = 7/2$.

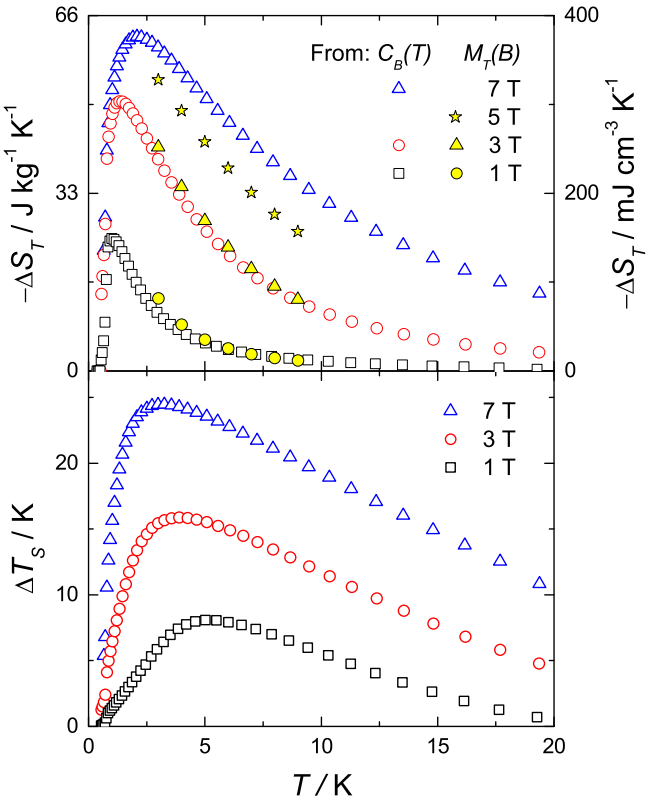

FIG. 5. (Color online) Top: Isothermal entropy increment ΔS_T for magnetic field increment, from zero to a given value, as labelled, computed from isothermal magnetization measurements and from heat capacity. Vertical axis reports units in Jkg^{-1}K^{-1} (left) and volumetric mJ/cm^{3}k^{-1} (right). Details about the absolute entropy in the text. Bottom: Adiabatic temperature increments, from zero field to a given value, as labeled, computed from heat capacity data. The abscissa is the initial temperature.

The total entropy $S(T,B)$ has been computed from the heat capacity at constant field, $C_B(T)$, as

$$S(T,B) = S(T_0,B) + \int_{T_0}^{T} \frac{C_B(T)dT}{T}. \quad (3)$$

The determination of the absolute entropies is usually made taking $T_0 = 0$, when $S = 0$, but the procedure is not always applicable, notably in the present case where the C_B data cannot be properly extrapolated to $T \to 0$ due to the existence of the magnetic anomaly at $T_N = 0.77$ K. Different procedures were followed to determine $S(T_0,B)$ for the curves at different fields, sketched in Fig. 4, bottom panel. For $B = 3$ T and 7 T, the experimental C_B data could be extrapolated down to $T = 0$ by a Schottky function (that matches very well the experimental C_B data up to 10 K), permitting to determine the absolute entropy at any other temperature. For $B = 0$, the magnetic heat capacity decreases as T^{-2} above T_N, becoming negligible at ca. 10 K, thus permitting to determine the phonon contribution to the entropy as $S_{\rm ph} \simeq AT^3/3$ on the basis of the aforementioned Debye specific heat term. The magnetic entropy was assumed to reach its maximum value of $R\ln(2s+1) = R\ln(8)$ for $s = 7/2$ at ca. $T = 10$ K. Finally, for the data collected for 1 T, none of the above approximations is valid. We estimated the magnetic entropy by a mean-field approximation in the paramagnetic state, i.e., precisely at 14.93 K (hence, very close to the $R\ln(8)$ limit). By so doing, the entropy extrapolates correctly to $T = 0$. With the aid of the so-obtained entropy curves for different fields, the quantities $\Delta S_T = S(T,B) - S(T,0)$ and $\Delta T_S = T(S,B) - T(S,0)$ were computed, with $T(S,B)$ being the inverse function of $S(T,B)$ for a given B. Figure 5 shows ΔS_T and ΔT_S as functions of the temperature at zero field.

The MCE has been estimated also from isothermal magnetization $M_T(B)$ data, collected using a MPMS-XL magnetometer from Quantum Design. The isothermal entropy increment ΔS_T under a given field variation was computed by integration of the well-known Maxwell relation:

$$\left(\frac{\partial S}{\partial B}\right)_T = \left(\frac{\partial M}{\partial T}\right)_B \Rightarrow$$

$$\Delta S_T \equiv S(T,B) - S(T,0) = \int_0^B \left(\frac{\partial M}{\partial T}\right)_B dB. \quad (4)$$

For the sake of brevity, we omit $M(T,B)$ data and plot the ΔS_T deduced from them in Fig. 5. The ΔS_T data derived from magnetization agree very well with those obtained from heat capacity and show a very large MCE, even higher than the benchmark gadolinium gallium garnet [21] and the record-holding gadolinium formate, which does not exceed $-\Delta S_T = 216.3$ mJ/cm^{3}K^{-1} for 7 T [4]. The large MCE can be explained by the combination of a large magnetic density,

weak magnetic interactions, small magnetic anisotropy, and modest lattice contribution to the heat capacity. This last item is an extra interesting feature of this material with regard to refrigeration as a small lattice heat capacity implies that the increase in the spin entropy following the demagnetization procedure is used almost entirely to absorb the heat from the sample that is to be cooled. The determination of ΔT_S from heat capacity requires careful evaluation of the absolute entropy for different fields. In the present case, the results are consistent with those obtained for ΔS_T, which are $\approx$1.7 times as large in volumetric units as those for $Gd(HCOO)_3$ [4]. This can be mainly attributed to the significantly larger density of Gd^{+3} spins in the phosphate. The mass density of $Gd(HCOO)_3$ is $\rho = 3.86$ gcm^{-3}, while that of $GdPO_4$ is $\rho = 6.06$ gcm^{-3}. In $GdPO_4$, all this results in the isothermal entropy increment reaching $-\Delta S_T = 62.0$ Jkg^{-1}K^{-1} $= 375.8$ mJ/cm^{3}K^{-1} and the adiabatic temperature increment reaching $\Delta T_S = 24.6$ K, for $T = 2.1$ K and a 7 T applied-field change (Fig. 5).

IV. DISCUSSION

We will now discuss the information collected thus far on the magnetic interactions and anisotropy parameters of $GdPO_4$. The spin Hamiltonian for the $s = 7/2$ Gd^{3+} spins can be written as

$$\mathcal{H} = \bar{g}\mu_B \mathbf{B}\cdot\mathbf{s} + \mathcal{H}_{\rm CF} + \mathcal{H}_{\rm dip} + \mathcal{H}_{\rm ex}, \tag{5}$$

that is the sum of the Zeeman interaction and the crystal-field (CF), dipolar, and superexchange interactions, respectively. The dipolar term can be readily computed for any spin configuration as a summation of moment-moment interaction terms up to a desired distance, when the r^{-3} dependence along with the antiferromagnetic configuration (for zero field) make the remainder negligible.

Rappaz *et al.* [22] determined the crystal-field terms by EPR. The four Gd^{3+} ions in the unit cell are divided into two pairs transforming into one another by the crystal symmetry operations, viz., the two ions of each pair being mutually related by inversion symmetry. Although the local site symmetry of the ninefold oxygen coordination of the Gd ions is very low, the EPR spectra could be quite successfully analyzed assuming orthorhombic $2/m$ or C_{2h} site symmetry (with three orthogonal principal axes). Accordingly, the EPR spectra were analyzed in terms of a crystal-field Hamiltonian $\mathcal{H}_{\rm CF} = \sum_{n,m} B_n^m O_n^m$, taking into account terms up to order $n,m = 6$. Here, the O_n^m terms are the well-known Stevens' operator equivalents, and the B_n^m terms are the associated crystal-field parameters [23]. For numerical convenience [24], B_n^m are often replaced by b_n^m, related as $b_2^m = 3B_2^m$, $b_4^m = 60B_4^m$ and $b_6^m = 1260B_6^m$. Five out of the nine B_n^m parameters were determined in the EPR experiments. Hereafter, we adopt the values reported for the $EuPO_4 : Gd^{3+}$ single crystal. It should be remembered that Eu is next to Gd in the periodic table, so no significant differences in the EPR signal are to be expected. Besides, the observed variation over the entire series of rare-earth elements analyzed is very small. In what follows, we replace the orthorhombic symmetric crystal-field Hamiltonian, written in terms of Stevens' operators, by a spin Hamiltonian ($H_{\rm SH}$) more commonly used in magnetic studies. Keeping only terms quadratic in the spin operators s_z and $s_{x,y}$

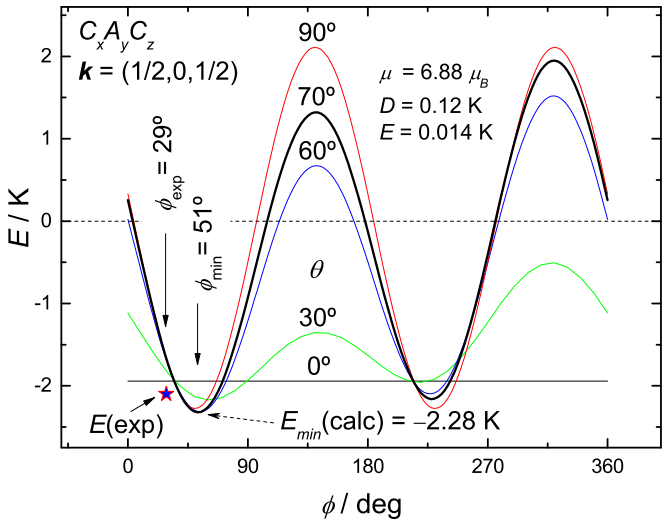

FIG. 6. (Color online) Free energy per particle considering anisotropy and dipolar interactions for the $C_xA_yC_z$ magnetic mode as a function of the azimuthal angle ϕ for different θ values defining the orientation of the moment at Gd1. The experimentally found magnetic energy is indicated.

(as justified by the fact that the measured 4^{th} and 6^{th} order terms are negligible) we may write the spin Hamiltonian in terms of the familiar parameters D and E as

$$\mathcal{H}_{\rm SH} = Ds_{z'}^2 + E\left(s_{x'}^2 - s_{y'}^2\right), \tag{6}$$

where $D = 3B_2^0 - [30X - 25]B_4^0 + [105X^2 - 525X + 294]B_6^0$ and $E = B_2^2 - [X + 5]B_4^2$, for $X \equiv s(s+1)$. Using the values given in Table II of Rappaz *et al.* [22], we obtain $D/k_B = +0.12$ K and $E/k_B = +0.014$ K.

As will be shown below, superexchange interactions in this compound are very weak and thus expected to play a very minor role. Neglecting superexchange and using the approximation given in Eq. (6) with anisotropy parameters (D and E) deduced from the EPR study, we have computed the crystal-field anisotropy energy $E_{\rm CF}$ and the dipolar energy $E_{\rm dip}$ of a distribution of magnetic moments with $\mu = 6.88\mu_B$ (as deduced here), mutually coupled by the dipole-dipole interaction for the four magnetic modes with $\mathbf{k} = (1/2,0,1/2)$ and for all possible orientations of the moment at the reference atom 1, with coordinates given explicitly in Table I. The orientations for the other atoms are determined by the symmetry operations given in Table II. Figure 6 shows the so-obtained results for the energy per particle $E = E_{\rm CF} + E_{\rm dip}$, where the dipolar term is calculated as [25]

$$E_{\rm dip} = \frac{1}{2N}\frac{\mu_0}{4\pi}\sum_{i=1}^{N}\sum_{j\neq i}\left(\frac{\mu_i\cdot\mu_j}{r_{ij}^3} - \frac{3(\mu_i\cdot\mathbf{r}_{ij})(\mu_j\cdot\mathbf{r}_{ij})}{r_{ij}^5}\right), \tag{7}$$

for each magnetic moment μ_i at $\mathbf{r}_i$ with every other magnetic moment μ_j at $\mathbf{r}_j$, and $\mathbf{r}_{ij} = \mathbf{r}_i - \mathbf{r}_j$. As can be seen, the minimum energy value $E_{\rm min}/k_B = -2.28$ K (for which $E_{\rm CF}/k_B = -0.62$ K and $E_{\rm dip}/k_B = -1.66$ K) is found to occur indeed for the configuration $C_xA_yC_z$, at values for the polar angles $\theta = 84^\circ$ and $\phi = 51^\circ$ that correspond to components along the

crystal axes $(\mu_x,\mu_y,\mu_z) = (5.65,0.72,5.48)\mu_B$, not far from the values observed above and listed in Table I and to the value of the total magnetic energy per particle obtained from the heat capacity experiments, i.e., $E_m/k_B = -2.2(1)$ K. The observed and calculated structures agree in the wave vector **k**, the magnetic mode, and fairly well in the direction of the moments, μ_y being the smallest component in both cases.

Several conclusions can now be drawn. First, the positive sign of D (and b_2^0) distinguishes the monoclinic rare-earth orthophosphate hosts from those having the tetragonal zircon structure, for which values for b_2^0 are found of similar magnitude but of negative sign [26]. The x', y', and z' axes correspond to the three principal axes of the local site pseudosymmetry. Thus, the positive $Ds_{z'}^2$ term establishes the local $x'y'$ plane as the easy plane for the Gd^{3+} magnetic moment, in which the y' axis is singled out as the most preferred by the positive E term. As noted by Rappaz *et al.* [22] and seen in Table II, the symmetry operations that transform one site into another are: (1) a 180° screw rotation with respect to the b axis, (2) a glide reflection on the ac plane, (3) inversion, and it is evident that the local x',y',z' system of axes of the sites should transform accordingly. The directions of the local y' and z' axes were found to lie on a cone making an angle $\theta = 67^\circ$ with the b axis (see Fig. 16 in Ref. [22]), whereas the projections of the local y' axes on the ac plane correspond to an azimuthal angle $\phi_{y'} = 41^\circ$ ($\pm 180^\circ$). Comparing this with the results of the neutron study, one may conclude therefore that the observed directions of the four antiferromagnetic sublattices are favored to large extent by the local crystal-field anisotropy, although E_{CF} is significantly smaller than E_{dip}.

This is explained as follows. Although the minimum dipolar energy $E_{dip}/k_B = -1.67$ K is large and occurs for $\theta = 90^\circ$ (corresponding to collinear moments aligned perpendicular to the b axis), E_{dip} increases only by about 0.1 K up to -1.55 K for the spin configuration corresponding to a minimum for the magnetic anisotropy (i.e., $\theta = 67^\circ$ and $\phi = 41^\circ$). The difference between these two values of E_{dip} is therefore much smaller than the corresponding difference in the anisotropy energy, i.e., 0.62 K. Consequently, although in a first approximation a collinear structure with the moments in the ac plane could be expected on the basis of the dipolar interaction solely, the presence of the anisotropy term produces a noncollinear configuration of lower energy. The net result is the experimentally determined four-sublattice structure with $\theta = 73^\circ$ and $\phi = 29^\circ$, close indeed to the values $\theta = 67^\circ$ and $\phi = 41^\circ$ favored by the local crystal-field site symmetries.

Second, since D is relatively large, the crystal-field splitting of the magnetic energy levels is relevant. Indeed, neglecting E at first approximation, the energy levels would be given by $E_i = g\mu_B s_z + D(s_z^2 - 21/4)$. Note that the positive sign of D implies that the $|\pm 1/2\rangle$ doublet lies lowest in energy. The highest-lying $|\pm 7/2\rangle$ doublet is then (in zero applied field) at $12D/k_B \approx 1.5$ K above the ground state, implying that it is appreciably depopulated in the temperature range above the ordering temperature $T_N = 0.77$ K. As a consequence, when analyzing the magnetic heat capacity tail observed above T_N in terms of the T^{-2} dependence expected in the high-temperature limit, only the data in the temperature range $T \gtrsim 3$ K should be taken into account. As is well known, above T_N, the magnetic heat capacity depends on temperature as $C_m/R \propto T^{-2}$. The expression for the coefficient of the limiting high-temperature T^{-2} term is given by the sum of the anisotropy, exchange and dipolar contributions as [24,27,28]

$$C_m T^2/R = [D^2 + 3E^2]s(s+1)(2s-1)(2s+3)/45k_B^2 + \mu_{\text{eff}}^2\left[\langle B_{i,\text{ex}}^2\rangle + \langle B_{i,\text{dip}}^2\rangle\right]/6k_B^2.$$

Here $\mu_{\text{eff}}^2 = g^2\mu_B^2 s(s+1)$, whereas $\langle B_{i,\text{ex}}^2\rangle$ and $\langle B_{i,\text{dip}}^2\rangle$ stand for the mean-square averages of the internal fields on a reference ion in the paramagnetic region due to, respectively, the exchange and the dipolar interaction. The exchange term is given by $g^2\mu_B^2\langle B_{i,\text{ex}}^2\rangle = \frac{1}{3}s(s+1)\sum_{i>j}[J_{xx}^2 + J_{yy}^2 + J_{zz}^2]$, the dipolar term is calculated as [25] $\langle B_{i,\text{dip}}^2\rangle = 2(\mu_0/4\pi)^2\mu_{\text{eff}}^2\sum_i r_{ij}^{-6}$, the summation being over all the other magnetic ions. As it turns out, the exchange contribution has to be very small compared to the anisotropy and dipolar contributions. After performing the necessary summations, we find the dipolar term to amount to 0.92 K^2. With the aforementioned values for D and E, the crystal-field part is calculated as 0.31 K^2, hence their sum amounts to $C_m T^2/R = 1.23$ K^2, whereas the experimentally found coefficient of the T^{-2} term is 1.1 K^2. Accordingly, the exchange term appears to be very small, probably negligible.

The same conclusion can in fact also be drawn from an analysis of the total magnetic energy, $E_m = E_{\text{ex}} + E_{\text{CF}} + E_{\text{dip}}$, involved in the magnetic ordering process, as can be obtained from the integration of the magnetic heat capacity curve, $\int C_m dT$, measured in zero field. As reported earlier [6], we obtain $E_m/k_B = 2.2(1)$ K experimentally. The minimum free energy configuration on the basis of the dipolar and anisotropy energies obtained above and shown in Fig. 6 corresponds to 2.28 K and thus accounts largely for the experimental total magnetic energy. Taken together, we may state that within the errors involved this leaves a maximum possible exchange contribution of the order of $z|J|S^2 \approx 0.1$ K, implying a $|J|/k_B$ of ≈2 mK only. It is noted that the behavior of the heat capacity of $GdPO_4$ resembles in several respects the results obtained for $GdCl_3 \cdot 6H_2O$ and $Gd_2(SO_4)_2$ [27], for which exchange contributions could also be disregarded. The value $|J|/k_B \leqslant 2$ mK found here is respectively 20 and 40 times less than the known values for the related compounds $GdAsO_4$ and $GdVO_4$, where the ordering is predominantly driven by the exchange interactions [6]. In all probability this should be ascribed to differences in the geometries and interatomic distances in the Gd-O-Gd superexchange paths in the monazite compound compared to the tetragonal zircon structure. A quantitative theoretical treatment of this problem is however outside the scope of the present paper.

Although exchange interactions are thus apparently negligible, it is of interest still to show that the symmetry involved in the long-range magnetically ordered structure of $GdPO_4$ would actually minimize their influence when present. This is most easily shown within the mean-field approximation to the exchange term in the Hamiltonian (5). Let us denote the Gd atom listed in Table I as Gd0. The six nearest neighbors Gd1, ..., Gd6 are at nearly equal distances, ranging from 4.00 Å to 4.24 Å. We define now the moment at site i as $\mu_i = -2\,\mu_B \mathbf{s}_i$. In the structure observed, these moments

TABLE III. Spins $\mathbf{s_1}, \ldots, \mathbf{s_6}$ of the six nearest neighbors, Gd1, ..., Gd6, with respect to the Gd atom listed in Table I, here renamed as Gd0. In the first column, "label" stands for the label used in Table II. Third, fourth, and fifth columns give the coordinates of the site and spin for the $CxAyCz$ configuration, respectively. The sixth column lists the distance and exchange constant. The last four columns list the rotation and translation applied in order to obtain the nearest neighbors from Gd0. The spin should be inverted when $tx + tz = odd$, due to the propagation vector $\mathbf{k} = (1/2,0,1/2)$.

Label in Table II	Atom	x,s_x	y,s_y	z,s_z	d(Å), J_i	Symm.	tx	ty	tz
(1)	Gd0	0.282	0.155	0.097	0	1	0	0	0
	$\mathbf{s}_0$	s_x	s_y	s_z					
(2)	Gd1	0.218	−0.345	0.403	4.00	2_1	0	−1	0
	$\mathbf{s}_1$	$-s_x$	s_y	$-s_z$	J_1				
(2)	Gd2	0.218	0.655	0.403	4.00	2_1	0	−1	0
	$\mathbf{s}_2$	$-s_x$	s_y	$-s_z$	J_1				
(3)	Gd3	−0.282	−0.155	−0.097	4.24	$\bar{1}$	0	0	0
	$\mathbf{s}_3$	$-s_x$	$-s_y$	$-s_z$	J_2				
(3)	Gd4	−0.718	−0.155	−0.097	4.00	$\bar{1}$	1	0	0
	$\mathbf{s}_4$	s_x	s_y	s_z	J_3				
(4)	Gd5	−0.218	0.345	−0.403	4.17	n	−1	0	−1
	$\mathbf{s}_5$	s_x	$-s_y$	s_z	J_4				
(4)	Gd6	0.782	0.345	0.597	4.17	n	0	0	0
	$\mathbf{s}_6$	s_x	$-s_y$	s_z	J_4				

are on four sublattices and we adopt the usual assumption that only interactions ($J_{ij}, i \neq j, j = 1$–6) between spins on different sublattices are operative. Neglecting any longer range interactions, the exchange term can then be written as

$$\mathcal{H}_{\text{ex}} = \sum_{j=1}^{6} J_{ij}\mathbf{s}_i \cdot \mathbf{s}_j \simeq \mathbf{s}_i \cdot \sum_{j=1}^{6} J_{ij}\mathbf{s}_j. \tag{8}$$

In principle mean-field theory applied to this problem could lead to several possible ordered antiferromagnetic structures. Instead, we impose the four-sublattice arrangement established by the combination of dipolar and CF interactions. Table III lists the components of the six nearest spin neighbors to a reference Gd0 spin for the $GdPO_4$ structure and the magnetic mode $C_xA_yC_z$ for $\mathbf{k} = (1/2,0,1/2)$. According to Table III, the ground-state molar exchange energy can be then be written as

$$\frac{2E_{\text{ex}}}{R} = Ps_{\perp}^2 + Qs_y^2 = (P-Q)s_{\perp}^2 + Qs^2, \tag{9}$$

where $P = 2(J_4 - J_1) + J_3 - J_2$, $Q = 2(J_1 - J_4) + J_3 - J_2$, and $\mathbf{s}_{\perp} = s_x\mathbf{u}_x + s_z\mathbf{u}_z$ is the projection of $\mathbf{s}$ on the ac plane, and the four intrasublattice exchange constants J_{ij} are denoted by $J_i, i = 1$–4.

A number of interesting conclusions can be extracted from Eq. (9). First, in the most general case, the exchange energy is seen to be the sum of differences between four similar exchange terms. Therefore, in case the J_i are similar in magnitude and in sign, the result will be quite small even for finite values for J_i. Indeed, in the special case $J_1 = J_2 = J_3 = J_4$, the exchange energy would even be exactly zero because of the symmetry of the $C_xA_yC_z$ mode with $\mathbf{k} = (1/2,0,1/2)$. Mean-field theory then predicts the system to remain in the disordered, paramagnetic state down to $T = 0$, similar to a frustrated antiferromagnet, such as the well-studied gadolinium gallium garnet [3]. However, in view of the known differences in the superexchange paths between the nearest neighbors this situation will not likely occur. Obviously, if the exchange interactions would have been substantial, i.e., of the same order as the dipolar interactions or the CF anisotropy energy, the system could have ordered in a completely different antiferromagnetic arrangement, for instance as found in the previously published Monte Carlo simulations [6].

V. CONCLUSIONS

We have determined the magnetic structure of $GdPO_4$, which undergoes a transition to a magnetically ordered state below $T_N = 0.77$ K. The present data unambiguously show the magnetic structure to be a four-sublattice compensated antiferromagnetic arrangement, which is found to be favored by the dipolar interaction in combination with the local crystal-field site symmetries at the four Gd^{3+} sites in the unit cell. The magnetic superexchange is found to be negligible compared to the dipolar and crystal-field energies, making this compound an interesting example of a dipolar antiferromagnet.

The magnetocaloric effect is found to exceed by a considerable margin the maximum values reported to date, as were measured for Gd formate [4]. $GdAsO_4$ and $GdVO_4$ have much higher T_N in spite of larger distances. Probably in these cases, the magnetic order is dominated by the exchange interaction. These compounds are worthy of further research. A proposed strategy to produce high magnetocaloric materials is to find high magnetic density compounds where dipolar, exchange, and anisotropy compete (rather than trying to make them very small, when the dipolar energy increases with the magnetic density in any case), preventing ordering down to very low temperatures.

ACKNOWLEDGMENTS

We are grateful to John Archer and Philippe Decarpentrie from ILL for technical assistance, and Jolanta Stankiewicz from ICMA for useful discussions. We acknowledge the ILL for the allocation of neutron beam time (experiment

5-41-372) and the Spanish MINECO for funding this research through Grant Nos. MAT2012-38318-C03-01 and MAT2013-44063-R. Research at the Oak Ridge National Laboratory for one author (L.A.B.) was sponsored by the U.S. Department of Energy, Basic Energy Sciences, Materials Sciences and Engineering Division.

[1] W. F. Giauque and D. P. MacDougall, Phys. Rev. **43**, 768 (1933).
[2] F. Pobell, *Matter and Methods at Low Temperatures* (Springer, Berlin, Heidelberg, New York, 2007).
[3] See, e.g., P. Schiffer, A. P. Ramirez, D. A. Huse, and A. J. Valentino, Phys. Rev. Lett. **73**, 2500 (1994); P. Schiffer, A. P. Ramirez, D. A. Huse, P. L. Gammel, U. Yaron, D. J. Bishop, and A. J. Valentino, *ibid.* **74**, 2379 (1995) and references to earlier works cited in these papers.
[4] G. Lorusso, J. W. Sharples, E. Palacios, O. Roubeau, E. K. Brechin, R. Sessoli, A. Rossin, F. Tuna, E. J. L. McInnes, D. Collison, and M. Evangelisti, Adv. Mater. **25**, 4653 (2013).
[5] C. Thiriet, R. J. M. Konings, P. Javorský, N. Magnani, and F. Wastin, J. Chem. Therm. **37**, 131 (2005).
[6] M. Evangelisti, T. G. Sorop, O. N. Bakharev, D. Visser, A. D. Hillier, J. J. Alonso, M. Haase, L. A. Boatner, and L. Jos de Jongh, Phys. Rev. B **84**, 094408 (2011).
[7] J. A. Blanco, J. I. Espeso, J. García Soldevilla, J. C. Gómez Sal, M. R. Ibarra, C. Marquina, and H. E. Fischer, Phys. Rev. B **59**, 512 (1999).
[8] J. S. Abell, J. X. Boucherle, R. Osborn, B. D. Rainford, and J. Sweizer, J. Magn. Magn. Mater. **31–34**, 247 (1983).
[9] V. F. Sears, P. J. Brown, and B. T. M. Willis, *International Tables for Crystallography*, Vol. C, edited by A. J. C. Wilson (Kluwer Academic Publishers, Dordrecht, 1992), p. 383.
[10] M. S. Lehmann, W. Kuhs, G. J. McIntyre, C. Wilkinson, and J. Allibon, J. Appl. Cryst. **22**, 562 (1989).
[11] D. F. Mullica, D. A. Grossie, and L. A. Boatner, Inorg. Chim. Acta **109**, 105 (1985).
[12] Y. Ni, J. M. Hughes, and A. N. Mariano, American Mineralogist **80**, 21 (1995).
[13] C. Wilkinson, H. W. Khamis, R. F. D. Stansfield, and G. J. McIntyre, J. Appl. Cryst. **21**, 471 (1988).
[14] G. J. McIntyre and R. F. D. Stansfield, Acta Cryst. A **44**, 257 (1989).
[15] P. Coppens, L. Leiserowitz, and D. Rabinovich, Acta Cryst. **18**, 1035 (1965).
[16] J. Rodrïguez-Carvajal, FULLPROF program. Institut Laue-Langevin (ILL), 2009; J. Rodrïguez-Carvajal, Physica B **192**, 55 (1993) (the FullProf Suite and corresponding documentation can be obtained from the web at http://www.ill.eu/sites/fullprof/).
[17] G. Bergerhoff, *International Tables for Crystallography*, Vol. C, edited by A. J. C. Wilson (Kluwer Academic Publishers, Dordrecht, 1992), p. 683.
[18] See Supplemental Material at http://link.aps.org/supplemental/10.1103/PhysRevB.90.214423 for details of the nuclear and magnetic structure determinations.
[19] E. F. Bertaut, in *Spin Configuratios of Ionic Structures: Theory and Practice*, Magnetism Vol. III, edited by G. T. Rado and H. Suhl (Academic Press, New York, 1963), Vol. 149.
[20] C. Thiriet, P. Javorský, and R. J. M. Konings, Solid State Commun. **134**, 409 (2005).
[21] A. M. Tishin and Y. I. Spichkin, *The Magnetocaloric Effect and its Applications* (IOP Publishing Ltd., Bristol and Philadelphia, 2003).
[22] M. Rappaz, M. M. Abraham, J. O. Ramey, and L. A. Boatner, Phys. Rev. B **23**, 1012 (1981).
[23] M. T. Hutchings, in *Solid State Physics*, Vol. 16, edited by F. Setiz and D. Turnbull (Academic Press, New York, 1964), p. 227.
[24] K. D. Bowers and J. Owen, Rep. Prog. Phys. **18**, 304 (1955).
[25] J. H. van Vleck, J. Chem. Phys. **5**, 320 (1937).
[26] M. Rappaz, L. A. Boatner, and M. M. Abraham, J. Chem. Phys. **73**, 1095 (1980).
[27] R. F. Wielinga, J. Lubbers, and W. J. Huiskamp, Physica **37**, 375 (1967).
[28] A. Abragam and B. Bleaney, *Electron Paramagnetic Resonance of Transition Ions* (Clarendon Press, Oxford, 1970), Appendix A.